Polymer 50 (2009) 2320–2327

Contents lists available at ScienceDirect

Polymer

journal homepage: www.elsevier.com/locate/polymer

Influence of soft segment composition on phase-separated microstructure of polydimethylsiloxane-based segmented polyurethane copolymers

Taeyi Choi [a], Jadwiga Weksler [b], Ajay Padsalgikar [b], James Runt [a,*]

[a] Department of Materials Science and Engineering, The Pennsylvania State University, University Park, PA 16802, USA
[b] AorTech Biomaterials, Dalmore Drive, Caribbean Park, Scoresby, VIC 3179, Australia

ARTICLE INFO

Article history:
Received 28 December 2008
Received in revised form
27 February 2009
Accepted 7 March 2009
Available online 25 March 2009

Keywords:
Polyurethane
Microstructure
Small-angle X-ray scattering

ABSTRACT

Segmented polyurethane block copolymers were synthesized using 4,4′-methylenediphenyl diisocyanate (MDI) and 1,4-butanediol (BDO) as hard segments and various soft segments derived from poly(hexamethylene oxide) (PHMO) and poly(dimethylsiloxane) (PDMS)-based macrodiols and mixtures thereof. The microstructure and degrees of phase separation were characterized using a variety of experimental methods. Copolymers synthesized with the PDMS macrodiol and from PDMS/PHMO macrodiol mixtures were found to consist of three phases: a PDMS phase; hard domains; and a mixed phase of PHMO, PDMS ether end group segments and some dissolved hard segments. Two models were used to characterize the small-angle X-ray scattering from these copolymers: pseudo two-phase and core–shell models. Analysis using both methods demonstrates that as the PDMS content in the soft segment mixture increases, the greater the fraction of hard segments involved in hard domains than are dissolved in the mixed phase. Findings from analysis of the carbonyl region of FTIR spectra are also in agreement with greater hard/soft segment demixing in copolymers containing higher PDMS contents.

1. Introduction

Segmented thermoplastic polyurethanes (PUs) with substantial strength, toughness and elasticity are used widely in a variety of applications. The versatility of this family of materials arises from the ease of changing segment chemistries and molecular weights, and hard/soft segment composition [1–4]. Historically, polyester, polyether, polycarbonate and poly(dimethylsiloxane) [PDMS] macrodiols have been utilized in PUs intended for biomedical applications [5–8]. In particular, PDMS-based PUs are receiving increasing attention by providing a combination of excellent biostability and mechanical properties [6,9–14].

A macrodiol mixture is generally used to achieve useful properties in PDMS-based polyurethanes [6,12,13,15], since adding a relatively hydrophilic (e.g. polyether) macrodiol along with a PDMS-based macrodiol has been found to provide improved compatibility between polar urethane hard domains and the nonpolar siloxane soft domains [10,15,16]. In the early research of Adhikari et al., PUs were synthesized having the same hydroxy-terminated PDMS and five different polyether polyols [in an 80/20 (PDMS/polyether) ratio], and containing 40 wt% hard segments [derived from 4,4′-methylenediphenyl diisocyanate (MDI) and 1,4-butanediol (BDO)] [6,15]. Among the various polyether comacrodiols investigated, polyhexamethylene oxide (PHMO) was determined to impart the most desirable mechanical properties [15].

Segmented polyurethanes prepared with mixed PDMS/PHMO [11] or PDMS/polytetramethylene oxide (PTMO) macrodiols [17] were reported to possess a three-phase microphase-separated structure: a siloxane phase, a hard segment phase, and an ether-rich phase containing dissolved or trapped hard segments. MDI/BDO copolymers containing PDMS and PHMO soft segments in an 80/20 ratio were found to exhibit excellent biostability and relatively low hardness, tensile and flexural moduli [6].

Although MDI/BDO-based PUs with an 80/20 ratio of macrodiols have been synthesized and characterized previously, the influence of changes in soft segment ratio on the microstructure and corresponding properties has not been explored. Extending our previous investigation of segmented PUs with mixed PDMS/PHMO soft segments in the usual 80/20 ratio [11], we synthesize in this study a series of PDMS/PHMO polyurethanes having a fixed hard segment content with selected PDMS/PHMO ratios, and investigate the corresponding phase-separated microstructure.

* Corresponding author.
E-mail address: runt@matse.psu.edu (J. Runt).

0032-3861/$ – see front matter © 2009 Elsevier Ltd. All rights reserved.
doi:10.1016/j.polymer.2009.03.024

2. Experimental section

2.1. Materials

PDMS/PHMO-based polyurethanes were synthesized from MDI and BDO as the hard segments, and a mixed macrodiol of α,ω-hydroxy-terminated PDMS and PHMO as the soft segments (see Fig. 1). MDI and BDO were purchased from Sigma Aldrich (98% purity) and α,ω-hydroxy-terminated PDMS and PHMO were synthesized by AorTech Biomaterials. The molecular weights of PDMS and PHMO are 1000 g/mol and 700 g/mol, respectively. The polydispersity indices of the two macrodiols were approximately 1.5 and the purities were greater than 97%. In previous DSC measurements, the α,ω-hydroxy-terminated PDMS macrodiol was found to exhibit two glass transition temperatures (T_gs), one at −105 °C arising from the siloxane segments and another at −8 °C from the ether end group segments [11]. The T_g of the PHMO macrodiol was found to be −35 °C.

The polyurethane copolymers were synthesized using a two-step bulk polymerization method [10,11] with systematic alteration of the proportion of the two macrodiols. A prepolymer was prepared by carefully adding MDI to a reaction vessel containing the mixed macrodiols, and BDO was subsequently added for chain extension. All copolymers investigated herein contain 60 wt% soft segments, and the ratio of PDMS to PHMO varies from 0/100, 20/80, 40/60, 60/40, 80/20 to 100/0. In subsequent discussion these copolymers are referred to as *0040*, *2040*, *4040*, *6040*, *8040* and *10040*; first two or three digits represent PDMS content in the soft segment mixture and the last two (*40*) represent the (fixed) hard segment content. The number average molecular weights of the synthesized copolymers range from 87,000 to 132,000 g/mol with a polydispersity of 1.6, measured by gel permeation chromatography relative to polystyrene standards. Films of 120–140 μm thickness were cast from 20 to 40% solutions of the polymers in *N*,*N*-dimethylacetamide (DMAc, Biolab Australia, minimum 99% purity) and heated at 55 °C for 16–18 h. The cast films were further dried under vacuum at 40 °C for another 24 h before evaluation.

2.2. Tapping mode atomic force microscopy [AFM]

The surface morphology of the *0040–10040* films was imaged using a DI multimode AFM in tapping mode with a low tapping force ($r_{sp} = 0.75–0.9$). $r_{sp} = A/A_0$ (set point amplitude/free amplitude of tip oscillation) and the free oscillation amplitude were set at 20 nm. Larger r_{sp} corresponds to smaller tapping forces.

2.3. Dynamic mechanical analysis

Dynamic mechanical analysis (DMA) was performed using a TA-Q800 DMA. DMA measurements were conducted at a heating rate of 3 °C/min and the frequency of 1 Hz in the tensile mode.

2.4. Differential scanning calorimetry [DSC]

DSC measurements were performed on a TA-Q1000 DSC. First and second heating scans were acquired from −100 to 250 °C at a rate of 10 °C/min, and the second heating scan followed fast cooling from 250 to −100 °C within several minutes to provide the same thermal history of all copolymers considered.

2.5. Wide-angle X-ray diffraction [WAXD]

Wide-angle X-ray diffraction patterns were collected on a Rigaku DMAX/rapid micro-diffractometer in transmission mode using a copper point focused source (1.54 Å) at 50 kV and 40 mA.

2.6. Fourier transform infrared spectroscopy [FTIR]

Transmission FTIR spectroscopy was conducted using a Nicolet 6700 FTIR spectrometer (Thermo Scientific). Films of *0040* through *10040* were dissolved in tetrahydrofuran to create a 2 wt% solution. The solutions were cast onto KBr windows and dried overnight at ambient conditions and dried further for 2 h at 80 °C under vacuum. Each sample was scanned 100 times averaged at a resolution of 2 cm^{-1}.

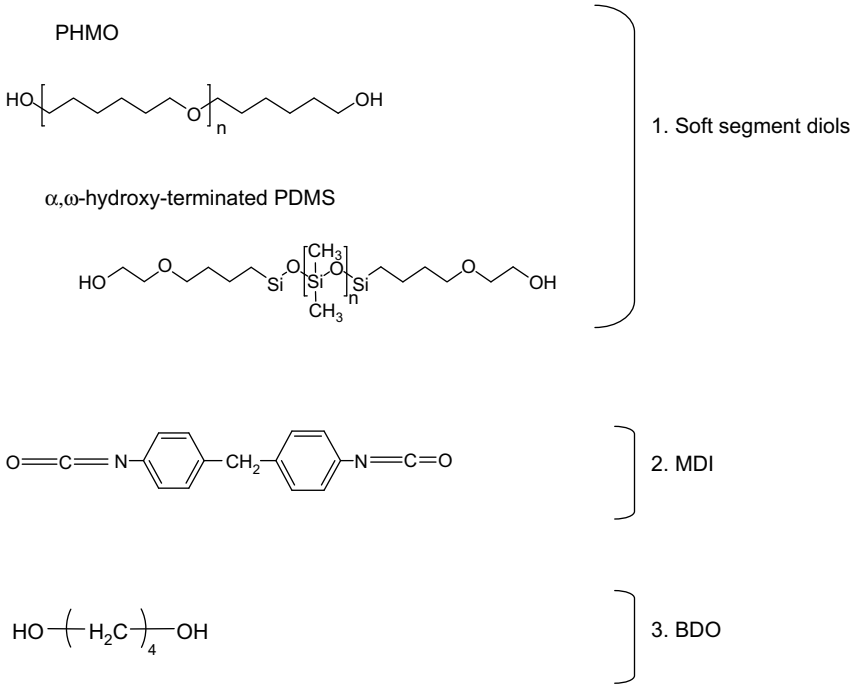

Fig. 1. Chemical structures of the components of the PDMS/PHMO-based polyurethanes under consideration.

2.7. Small-angle X-ray scattering [SAXS]

SAXS data were collected on a Molecular Metrology SAXS instrument using a CuKα radiation ($\lambda = 0.154$ nm) and a two-dimensional multi-wire detector. The sample-to-detector distance was 1.5 m. Absolute scattered intensities were calculated by comparing the spectra of the samples to those of a pre-calibrated polyethylene (S-2907) secondary standard [18].

3. Results and discussion

3.1. Phase morphology

To examine the phase morphology of *0040* through *10040*, tapping mode AFM phase images were acquired at low tapping forces (Fig. 2). Based on prior studies, the bright regions (yellow[1]) represent hard domains and the darker (brown) represent soft phase. These images suggest that the hard domains are not continuous, in contrast to some other tapping mode AFM reports of polyurethanes or polyurethaneureas having more or less continuous phases [19–21]. The mean size of the hard domains in the phase images is approximately 10 nm and there is no apparent difference in morphology on changing soft phase composition.

3.2. Phase transitions

Fig. 3 displays the storage moduli and mechanical tan δ as a function of temperature. A low temperature process ($T_{\alpha 1}$) is observed at −95 °C: it does not change significantly in location but its magnitude increases with PDMS content, and is assigned to segmental motion in the PDMS phase. A second α process ($T_{\alpha 2}$) is observed at higher temperatures and increases systematically from 5 to 20 °C with increasing PDMS fraction in the soft segment. This transition is associated with the segmental relaxation of a second (mixed) soft phase [2,11]. $T_{\alpha 2}$ increases with PDMS soft segment content, arising from the relative decrease in low T_g PHMO compared to higher T_g PDMS ether end group segments. The α_2 process also systematically broadens and decreases in magnitude with increasing PDMS soft segment content, the latter due to the reduction in overall polyether content. Similar behavior has also been reported for PDMS/PTMO-based polyurethanes with varying soft segment composition [17]. *0040* (without PDMS soft segments) consists of 'only' two phases: (1) hard domains (no hard phase transitions were observed in the DMA due to the limitation on making measurements at higher temperatures due to specimen stretching), and (2) a soft phase consisting of PHMO and dissolved hard segments.

Between about −80 and −20 °C, the storage moduli (Fig. 3a) decrease with increasing PDMS soft segment content, since the PDMS soft segments are above $T_{\alpha 1}$. However, above $T_{\alpha 2}$ (e.g. at 25 °C), the copolymers with higher PDMS contents exhibit higher E'. This arises from the greater degree of hard segment demixing for the higher PDMS containing copolymers, which will be discussed in Section 3.4.

Representative DSC thermograms corresponding to the first heating of the as-prepared copolymer films (aged at room temperature over a period of at least a month) are presented in Fig. 4a, and those of the copolymers rapidly cooled to low temperatures and immediately reheated are shown in Fig. 4b.

A T_g is evident near −20 °C in Fig. 4a and is associated with the mixed phase of PHMO, the ether end group segments of PDMS, and dissolved hard segments [11]. This assignment is consistent with the increase in the heat capacity change (ΔC_p) at T_g with increasing PHMO content in the soft segment. For *0040*, this transition represents the T_g of the mixed phase of PHMO and dissolved hard segments.

An endotherm is observed at ~60 °C in the first heating and has been proposed previously to correspond to the ordering of single ('lone') MDIs [15], but it is not at all clear what the driving force for such a process would be. 60 °C is near where the T_g of hard domains composed of oligomeric MDI–BDO might be expected. Broad endothermic transitions occur around 140–180 °C and the origin of similar transitions in PUs has been debated for many years. The circles in Fig. 4a represent the temperatures at which the scattering intensity disappears in SAXS experiments on *8040* and *10040* conducted as a function of temperature [22]. These points correspond to the approximate microphase mixing (or separation, on cooling) temperature (T_{MST}). Although the PDMS and hard segments are quite different chemically, the relatively low molecular weight of the segments and the 'compatibilizing' effect of polyether segments lead to solubility of the components at sufficiently high temperatures. This observation also agrees well with the disappearance of the absorbance of hydrogen-bonded carbonyls in temperature-controlled FTIR experiments, which will be discussed in the next section. The absence of crystallinity (see below), the disappearance of the SAXS scattering peak at elevated temperatures, and the FTIR results strongly suggest that the broad endotherm observed in DSC experiments of the PDMS/PHMO copolymers is associated at least partly, perhaps completely, with mixing of the unlike segments on heating. A more detailed discussion can be found in ref. [22].

The resulting thermograms after rapid cooling the copolymers to low temperatures are displayed in Fig. 4b. A T_g is observed near −15 °C and ΔC_p decreases as polyether content is reduced. An exotherm near ~40 °C follows T_g for the *0040*, *2040* and *4040* copolymers, whose magnitude decreases with increasing PDMS soft segment content. The origin of this transition is not clear, although it is not associated with crystallization of the hard or soft segments. Since these specimens have been very rapidly cooled from the single phase to two-phase state, we propose that unlike segment demixing is partially inhibited during rapid cooling of the PHMO soft segment rich copolymers, and this degree of phase separation is kinetically trapped below the soft phase (or mixed soft phase) T_g. On subsequent heating above the (mixed) soft phase T_g, segment mobility is enhanced and demixing continues, resulting in an exothermic response.

As shown in Fig. 5, X-ray diffraction patterns of the original aged films do not exhibit any crystalline diffraction peaks, but display characteristic amorphous halos at $2\theta = 12°$ (arising from the phase-separated PDMS segments) and at $2\theta = 20°$ (from non-PDMS segments). The behavior clearly demonstrates the phase-separated nature of the PDMS segments at room temperature. The amorphous halos arising from the siloxane segments increase in intensity gradually, while the other amorphous halos decrease, with increasing the PDMS content, as would be expected.

3.3. Hydrogen bonding by FTIR spectroscopy

In order to compare the FTIR spectra of the copolymers, we first normalized all to the absorbance of the N–H stretching vibration at 3325 cm^{-1} [23]. The PUs in this study have the same hard segment chemistry and content, and the N–H stretching peak should consequently have the same intensity for each. We then compared the relative absorbance of strongly hydrogen-bonded, loosely hydrogen-bonded, and "free" (non-hydrogen-bonded) carbonyl groups in the different materials, based on the idea that the quantity of hydrogen-bonded carbonyls can be related to the extent of hard segment bonding in hard domains [2,24]. A greater fraction

[1] For interpretation of the references to colour in this text, the reader is referred to the web version of this article.

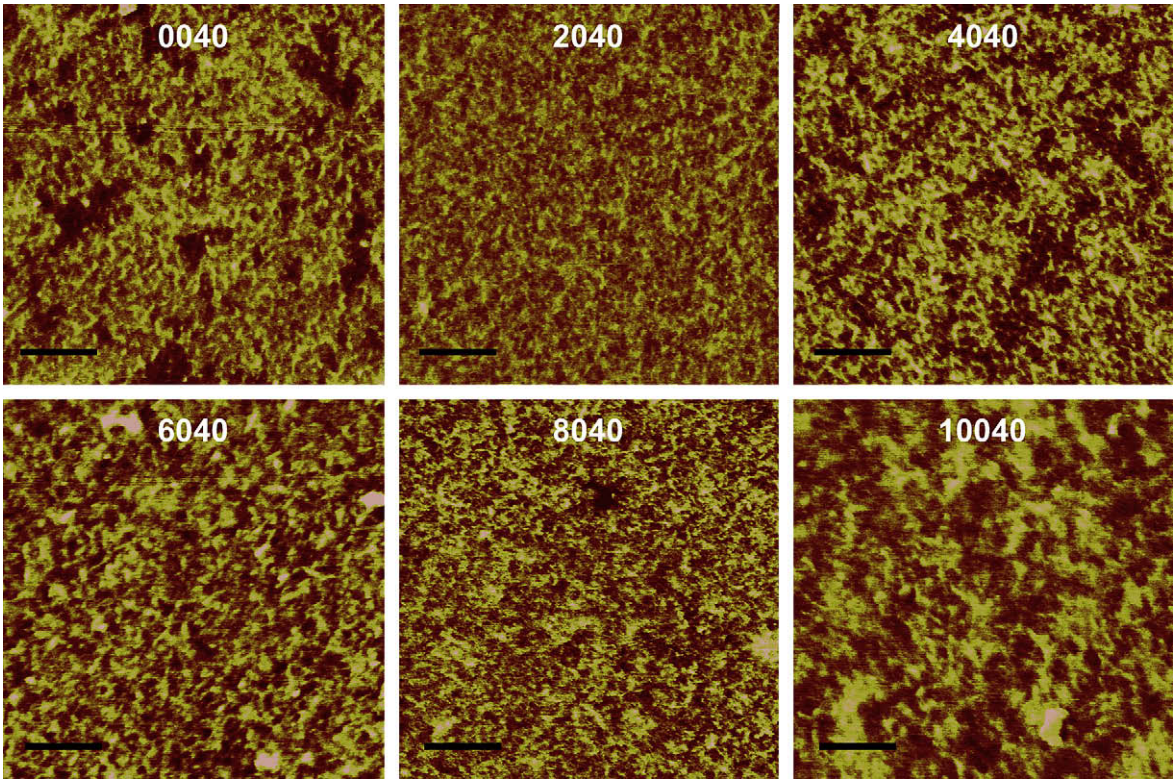

Fig. 2. AFM tapping mode phase images of PDMS/PHMO-PU surfaces using $r_{sp} = 0.75–0.9$. Scan size = 500 nm × 500 nm, the scale = 20°, and the scale bar on the images = 100 nm.

of H-bonded carbonyls would be expected to correlate with greater degree of hard domain formation. However, we cannot directly compare the forthcoming SAXS results for degree of microphase separation with those from FTIR, since the films used in the FTIR experiments are relatively thin and the observed behavior is not necessarily representative of the bulk (as evaluated by SAXS). In addition, the sample preparation procedure for FTIR spectroscopy is somewhat different from that of specimens used in the SAXS experiments.

The carbonyl region (from 1650 cm^{-1} to 1780 cm^{-1}) for each copolymer is displayed in Fig. 6. From previous studies, it has been well established that strongly hydrogen-bonded carbonyls are responsible for the absorbance at 1703 cm^{-1}, free (non-bonded) carbonyls for that at 1733 cm^{-1} and, although not so evident in Fig. 6, loosely hydrogen-bonded carbonyls (disordered hydrogen-bonded species) exhibit an absorbance near 1715 cm^{-1} [2,25]. This region was fit with three Gaussian–Lorentzian functions, resulting in the locations and areas of each of these bands. The areas of three bands are obtained; A_F is the area associated with free carbonyls, A_L that associated with loosely H-bonded carbonyls, and A_S that associated with strongly H-bonded carbonyls (not shown). To calculate and compare the effective numbers of H-bonded carbonyls, $A_L' = A_L/1.71$ and $A_S' = A_S/1.71$ were acquired, where 1.71 is the relative absorptivity of H-bonded carbonyls [25], and the total area is $A_T = A_F + A_L' + A_S'$. The relative absorbance fractions of the three carbonyl species are displayed in Table 1. With increasing PDMS soft segment content (see also Fig. 6), the area fraction of strongly H-bonded carbonyls increases while the fraction of free carbonyls decreases, indicating a decrease of unlike segment mixing. In other words, when there is more PDMS in the soft segment mixture, a larger fraction of carbonyl groups participates in strong hydrogen bonding with the N–H groups in the hard domains, rather than residing in a non-H-bonded condition in the soft phase. These findings are consistent with changes in degrees of phase separation estimated from SAXS experiments, which will be discussed in the next section.

In addition, we conducted temperature-controlled FTIR experiments on *8040* and *10040* from 20 °C to 200 °C in 20 °C increments (Fig. 7). At room temperature, the absorbance at ~1700 cm^{-1} is relatively intense and it gradually decreases and moves to higher frequency with increasing temperature, and this corresponds to a reduction in strongly H-bonded C═O. At the same time there is a corresponding increase in loosely H-bonded C═O with increasing temperature. The absorbance at ~1735 cm^{-1} moves to higher wave numbers and increases in absorbance with increasing temperature. These findings clearly demonstrate that most of the strongly H-bonded carbonyl groups become loosely bonded and the fraction of non-H-bonded carbonyls increases with increasing temperature.

3.4. Degrees of phase separation

Background corrected SAXS spectra of *0040* through *10040* films of ~0.8 mm thickness are displayed in Fig. 8. The peak position (q_{max}) is inversely related to the mean spacing between hard domains (d), $d = 2\pi/q_{max}$. The interdomain spacing decreases slightly with increasing PDMS soft segment content, as shown in Table 2.

Degrees of microphase separation are obtained by using the ratio of the experimental electron density variance to the theoretical electron density variance (i.e. the value calculated for the hypothetical case of complete phase separation) $[\Delta\overline{\eta}^{2\prime}/\Delta\overline{\eta}_c^2]$ [26–28]. The experimental electron density variance ($\Delta\overline{\eta}^{2\prime}$) is determined from the background corrected SAXS data [11]:

$$\Delta\overline{\eta}^{2\prime} = cQ = c\int\{I(q) - I_b(q)\}q^2\,dq \qquad (1)$$

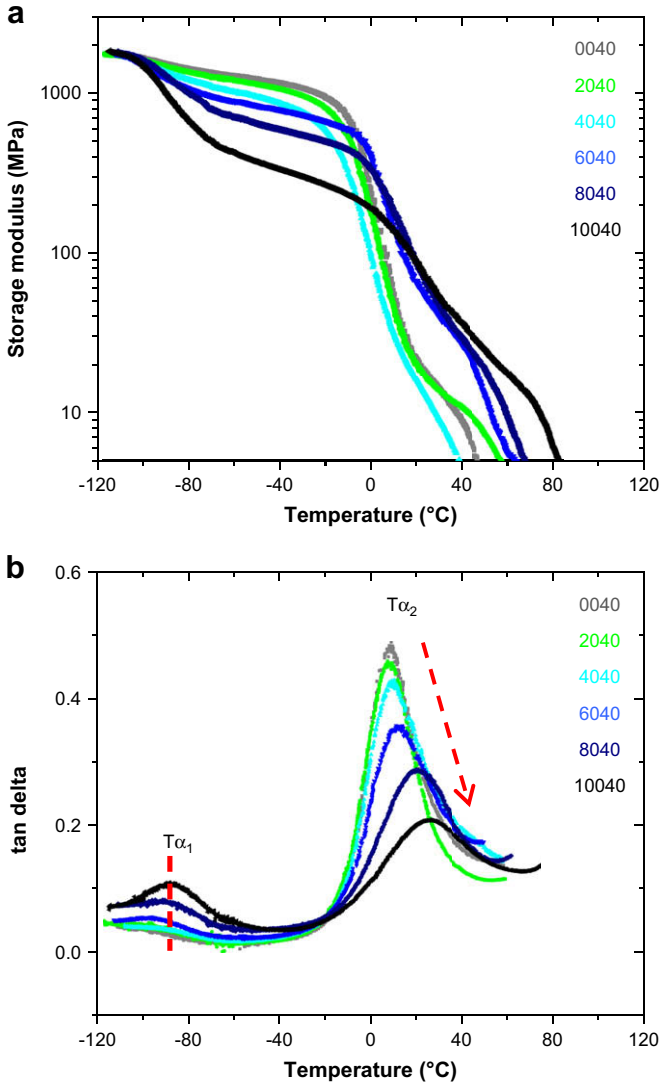

Fig. 3. (a) DMA storage modulus vs. temperature at 1 Hz and (b) the corresponding tan δ plot.

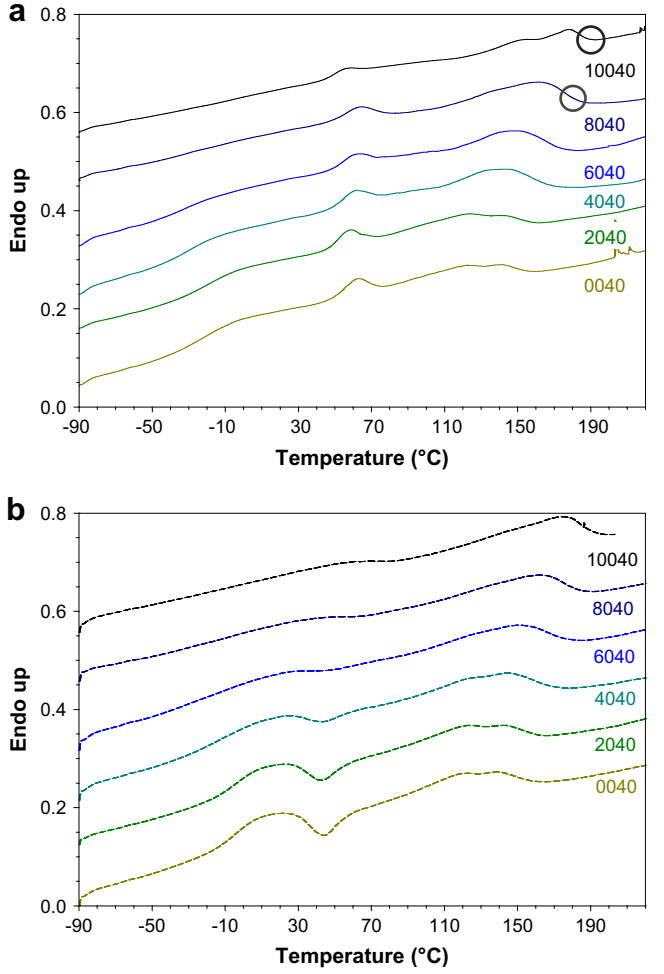

Fig. 4. Thermograms from DSC measurements: (a) from the first heating and (b) from the second heating after fast cooling.

where Q is the invariant (integrated intensity) and the constant c is

$$c = \frac{1}{2\pi^2 i_e N_{av}^2} = 1.76 \times 10^{-24} \left(\mathrm{mol}^2/\mathrm{cm}^2\right). \quad (2)$$

The symbol i_e refers to Thompson's constant for the scattering from one electron (7.94×10^{-26} cm^2) and N_{av} is Avogadro's number. The experimental electron density variances are summarized in Table 2. The theoretical electron density variances ($\Delta\overline{\eta}_c^2$) were calculated assuming complete hard and soft segment segregation, and assuming sharp boundaries between hard and soft domains, and are defined as [29]

$$\Delta\overline{\eta}_c^2 = \phi_{hs}\phi_{ss}(\eta_{hs} - \eta_{ss})^2 = \phi_{hs}(1 - \phi_{hs})(\eta_{hs} - \eta_{ss})^2, \quad (3)$$

where ϕ_{hs} and ϕ_{ss} are the volume fractions of the hard segments and soft segments in hypothetical completely phase-separated copolymers, respectively, and η_{hs} and η_{ss} are the electron densities of completely segregated hard and soft phases, respectively.

First, to determine the degree of unlike segment segregation for *0040*, the theoretical electron density variance was calculated from a two-phase model having a hard phase and soft polyether phase with dissolved 'lone' MDIs [30]. The calculated volume fractions

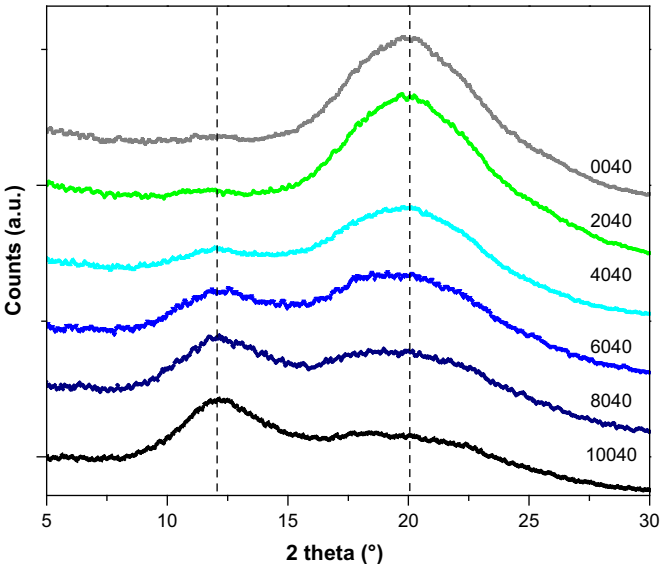

Fig. 5. WAXD patterns acquired by CuKα radiation ($\lambda = 1.54$ Å) for PDMS/PHMO-PUs: *0040* (top) through *10040* (bottom).

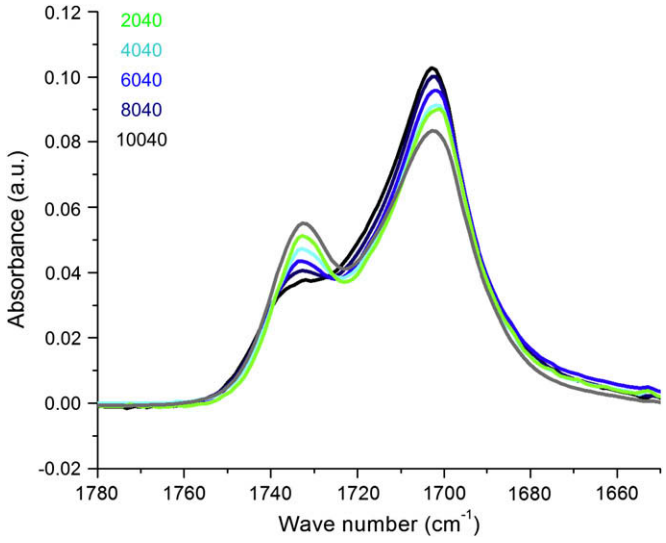

Fig. 6. FTIR spectra in the C=O stretching region from 1650 to 1780 cm^{-1}.

from the stoichiometry and the electron densities of the two hypothetical phases are summarized in Table 3, and the calculated theoretical electron density variance of *0040* is 4.55 $(mol\ e^-/cm^3)^2$. The experimental electron density variance of *0040* derived from the experimental scattering intensity is 1.56 $(mol\ e^-/cm^3)^2$, and the corresponding degree of phase separation is 0.34. This value of 0.34 is very near that obtained for PTMO-based polyurethanes with 40 wt% hard segments in ref. [2] (0.29). To compute the theoretical electron density variances of the three-phase *2040* through *10040* copolymers, we apply two models: a pseudo two-phase model [31,32] and a core–shell (Yarusso–Cooper) model [33–35].

3.4.1. Pseudo two-phase model

As noted earlier, PDMS/PHMO soft segment PUs consist of three phases: a PDMS phase, hard domains composed of hard segments, and a mixed phase of PHMO, the ether end groups of PDMS and some dissolved hard segments. To simplify the estimation of theoretical electron density variances for *2040–10040*, we first applied a *pseudo two-phase model*. The assumption was made in this case that only 'lone' MDIs are dissolved in the hypothetical polyether mixed phase, and longer hard segments are involved only in the hard phase. In order to justify applying a pseudo two-phase model to PDMS/PHMO PUs, we first calculated the hypothetical electron densities (η_i) and volume fractions (ϕ_i) of the three 'pure' phases, and compared the average electron density with that of each phase. The calculated electron densities are displayed in Table 3, and details of the calculations are provided in refs. [2,11]. Electron densities of the polyether soft phase were determined from the stoichiometry, the mass density of the components, and the number of electrons.

Since the average electron densities (η_{avg}) are similar to both the electron densities of the siloxane (η_1) and polyether mixed phases (η_3), the siloxane and mixed phase can be considered to be one soft segment phase for the purposes of this model. Therefore, the *hard domains (composed only of hard segments)* and a *soft phase containing the remainder of the segments (+lone MDIs)* are the two components considered in the pseudo two-phase model.

Table 1
Curve fitting results of the C=O stretching regions of the room temperature FTIR spectra of the *0040* through *10040* polyurethanes.

	1733 cm^{-1}	1715 cm^{-1}	1702 cm^{-1}
	A_F/A_T	A_L'/A_T	A_S'/A_T
0040	0.37	0.08	0.58
2040	0.30	0.08	0.62
4040	0.28	0.11	0.61
6040	0.25	0.10	0.65
8040	0.24	0.11	0.65
10040	0.21	0.12	0.67

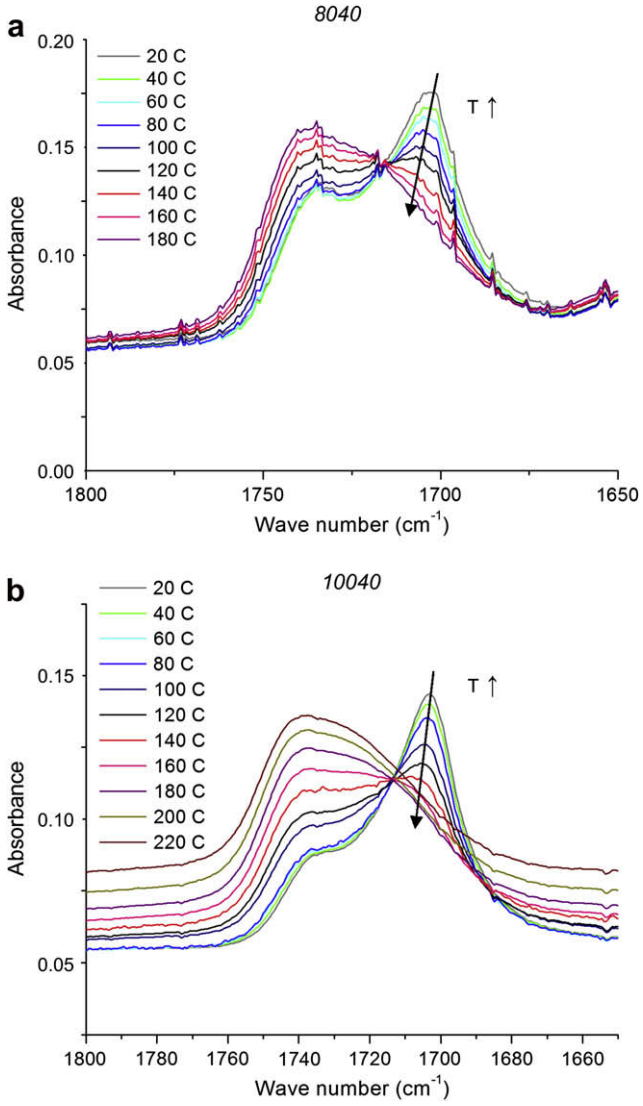

Fig. 7. FTIR spectra of *8040* and *10040* as a function of temperature from 20 to 180 °C (or 220 °C).

It is important to note that degrees of phase separation calculated with this model are defined differently from those determined for the two-phase *0040* (no PDMS): they denote what fraction of hard segments is involved in the hard phase, with the remainder residing in the soft phase. As shown in Table 2, the degrees of phase separation from the pseudo two-phase model increase from 0.3 for *2040* to 0.5 for *10040* (i.e. with increasing PDMS content). When there are more PDMS segments in the soft segment mixture, a larger fraction of hard segments are dissolved in hard domains, rather than being mixed with ethers in the soft phase. Since *0040–10040* have the same amount of hard segments, a greater number of hard segments phase separate into hard domains when PDMS soft segments dominate the soft segment composition.

3.4.2. Core–shell model

The second model used for analyzing the experimental SAXS spectra is core–shell (Yarusso–Cooper) modified hard-sphere

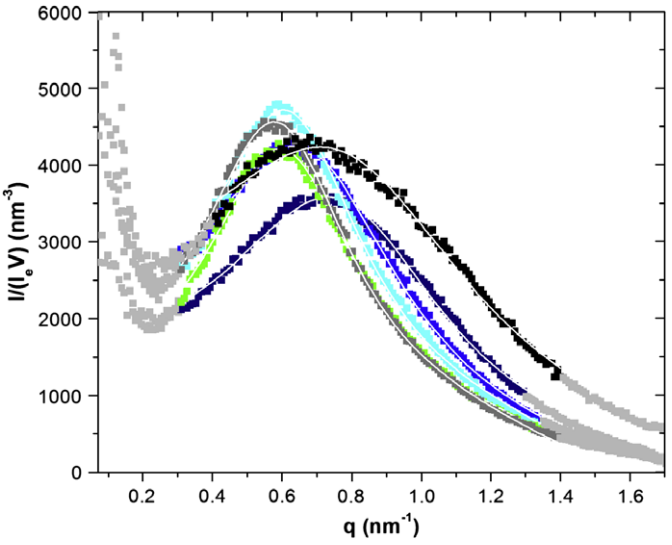

Fig. 8. Background corrected SAXS intensities and the curves (white) fitted by the core–shell model for (■) *0040*; (●) *2040*; (▲) *4040*; (▼) *6040*; (◆) *8040*; (◄) *10040*. The light gray data points at both high and low q were not used in the fitting.

scattering model. The core–shell model was originally designed for fitting the scattering of ionomer aggregates in a polymer matrix [33–35]. The model is applied by fitting the scattering curves with an expression for the scattering intensity [11,35]:

$$I(q) = I_e(q)V\frac{1}{V_p}F^2(q)\frac{1}{1+(8V_{ca}/V_p)\cdot\varepsilon\cdot\Phi(2qR_{ca})} \quad (4)$$

where $I_e(q)$ is the intensity scattered by a single electron, V the volume of the sample illuminated by the X-ray beam, V_p the average sample volume per particle, ε is a constant ~ 1, $V_{ca} = (4/3)\pi\cdot R_{ca}^3$ where $2R_{ca}$ is the closest approach distance between two domains, and $F(q) = \Delta\eta_1\cdot V_1\Phi(qR_1)$ is the structure factor of the scattering particle. The difference in electron density ($\Delta\eta_1$) between the scattering cores and the surrounding matrix is determined in the fitting by

$$\Delta\eta_1 = \eta_1 - \eta_2 \quad (5)$$

where phase 1 is composed of the siloxane units only (matrix) and phase 2 of scattering particles (cores), and V_1 is the volume of a scattering aggregate [11]. The other terms are defined as $\Phi(x) = 3((\sin x - x\cos x)/x^3)$ and $V_1 = (4/3)\pi\cdot R_1^3$, where R_1 (the radius of a scattering core) is smaller than R_{ca}.

The resulting fitted curves (white) are displayed on the experimental SAXS intensities in Fig. 8. Table 4 lists the best-fit parameters. In addition, the calculated differences in electron density assuming complete phase separation of hard, siloxane and the mixed phases,

Table 2
Interdomain spacing (d), experimental electron density variances ($\Delta\overline{\eta}^{2\prime}$), theoretical electron density variances ($\Delta\overline{\eta}_c^2$) and degrees of phase separation calculated from $\Delta\overline{\eta}^{2\prime}/\Delta\overline{\eta}_c^2$ for the pseudo two-phase model.

	$d = 2\pi/q_{max}$ (nm)	$\Delta\overline{\eta}^{2\prime} = cQ\times 10^3$ $(\text{mol e}^-/\text{cm}^3)^2$	$\Delta\overline{\eta}_c^2\times 10^3$(HS/rest) $(\text{mol e}^-/\text{cm}^3)^2$	Deg. phase separation
0040	11.4	1.56	4.55[a]	0.34[a]
2040	10.7	1.51	4.82	0.31
4040	10.7	1.75	4.67	0.37
6040	9.5	1.95	4.51	0.43
8040	8.9	2.01	4.35	0.46
10040	9.2	2.11	4.19	0.50

[a] Theoretical electron density variance and calculated degree of phase separation of *0040* are based on a *real* two-phase model.

Table 3
Theoretical volume fractions and electron densities for the ith phases in the copolymers; $i = 1$ for PDMS only, $i = 2$ for hard segments only, $i = 3$ for PHMO, PDMS ether end group segments and lone MDIs.

	η_1 $(\text{mol e}^-/\text{cm}^3)$	ϕ_1	η_2 $(\text{mol e}^-/\text{cm}^3)$	ϕ_2	η_3 $(\text{mol e}^-/\text{cm}^3)$	ϕ_3	η_{avg}
0040	0.569	0.00	0.733	0.23	0.566	0.72	0.579
2040	0.569	0.14	0.733	0.25	0.571	0.57	0.583
4040	0.569	0.25	0.732	0.26	0.578	0.44	0.585
6040	0.569	0.35	0.731	0.26	0.593	0.33	0.590
8040	0.569	0.44	0.731	0.27	0.609	0.24	0.591
10040	0.569	0.51	0.730	0.27	0.643	0.16	0.593

$\Delta\eta_{hs}$ and $\Delta\eta_m$, are provided in Table 4. The electron density difference between the siloxane matrix and the hard domain cores is:

$$\Delta\eta_{hs} = \eta_1 - \eta_{hs} \quad (6)$$

where *phase 1* is defined as the siloxane matrix and *phase hs* contains hard segments only. The difference in electron density between the siloxane matrix and the shell composed of PHMO, PDMS end group segments and lone MDIs is:

$$\Delta\eta_m = \eta_1 - \eta_m \quad (7)$$

where *phase 1* is siloxane matrix and *phase m* (for mixed) consists of PHMO, the ether end segments of the PDMS macrodiol, and lone MDIs. These two values are calculated using the electron densities in Table 3 and the units are converted from molar quantities $(\text{mol e}^-/\text{cm}^3)$ to atomic units (nm^{-3}).

In order to determine mean dimensions of the core (hard domains) and shell (the mixed phase) from this model, the electron density difference ($\Delta\eta_1$) between the core and the matrix must be fixed to be the same as the calculated electron density difference ($\Delta\eta_{hs}$) between the hard domains and the siloxane matrix. However, as noted previously [11], for PDMS/PHMO PUs containing more than 40% hard segments, the nonlinear least-squares regression provides adequate fits only when varying $\Delta\eta_1$ as a fitting parameter, and when the resulting $\Delta\eta_1$ lies between $\Delta\eta_{hs}$ and $\Delta\eta_m$. (We used a revised value for $\Delta\eta_m$ for *8040*, different from that reported in ref. [11].)

By comparing the fitted electron density difference ($\Delta\eta_1$) with the two calculated electron density differences ($\Delta\eta_{hs}$ and $\Delta\eta_m$), we determine the volume fraction of hard segments, Φ_{hs}, involved in the hard domains using:

$$\Delta\eta_1 = \Phi_{hs}\Delta\eta_{hs} + (1-\Phi_{hs})\Delta\eta_m \quad (8)$$

Calculated Φ_{hs} are displayed in Table 4 (Φ_{hs} for *8040* is slightly different than reported previously [11] due to the revised value of $\Delta\eta_m$). The volume fraction of hard segments residing in hard domains increases from approximately 0.4 to 0.75 as PDMS content increases. As was the case for the pseudo two-phase model, these results demonstrate that a higher volume fraction of hard segments is involved in hard domains when the soft segment mixture contains a greater fraction of the PDMS macrodiol.

Table 4
Fitting parameters (fit) obtained from the core–shell model, and the calculated (cal) electron density differences, the dimensions of the hard domains and the volume fraction of hard segments.

	Fit	Cal	Cal	Cal	Fit	Fit	Fit	Fit
	$\Delta\eta_1$ (nm^{-3})	$\Delta\eta_{hs}$ (nm^{-3})	$\Delta\eta_m$ (nm^{-3})	Φ_{hs}	R_{ca} (nm)	R_1 (nm)	$V_p^{1/3}$ (nm)	V_1 (nm^3)
2040	41	99	1	0.41	4.4	2.3	10.7	50.7
4040	45	98	5	0.43	4.3	2.3	10.6	50.4
6040	51	98	15	0.44	3.8	2.2	10.8	43.1
8040	63	97	24	0.53	3.5	1.9	9.5	26.6
10040	84	97	45	0.75	3.2	1.8	10.2	23.9

4. Summary

A series of segmented PUs were synthesized with two macrodiols and mixtures thereof, at a fixed MDI/BDO hard segment content. Characterization of the microstructure and unlike segment demixing were conducted with a variety of experimental probes. Findings from DMA and DSC experiments demonstrate that the soft phase of the two-phase copolymer *0040* (having only PHMO soft segments) consists of PHMO and some dissolved hard segments. The other five samples in the series were observed to exhibit three phases: a siloxane phase, a hard segment phase, and a mixed phase consisting of PHMO, PDMS ether end group segments and some dissolved hard segments. From FTIR spectroscopy, the fraction of strongly hydrogen-bonded carbonyl groups, which is correlated with hard domain formation, increases with increasing PDMS/PHMO content in the copolymers. Two models were used to analyze experimental SAXS data from the copolymers, the pseudo two-phase and core–shell models. From the core–shell model, we calculated the volume fraction of hard segments involved in the hard and mixed phases from the electron density difference between the scattering core, shell and the matrix. The analysis of the SAXS data with both the pseudo two-phase and core–shell models demonstrates that as the PDMS/PHMO ratio in the soft segment mixture increases, more hard segments become involved in hard domains and less are dissolved in the mixed phase. The PUs containing a greater fraction of PDMS exhibit a greater degree of hard/soft segment demixing.

Acknowledgments

The authors would like to thank Dr. Rebeca Hernandez for helpful discussions on SAXS analysis, Kevin Masser for his assistance with WAXD experiments, and Profs. Janna Maranas and Evangelos Manias for use of their DSC and AFM, respectively.

References

[1] Adhikari R, Gunatillake PA, Bown M. J Appl Polym Sci 2003;90:1565–73.
[2] Hernandez R, Weksler J, Padsalgikar A, Choi T, Angelo E, Lin JS, et al. Macromolecules 2008;41:9767–76.
[3] Martin DJ, Meijs GF, Gunatillake PA, Yozghatlian SP, Renwick GM. J Appl Polym Sci 1999;71:937–52.
[4] Takahara A, Coury AJ, Hergenrother RW, Cooper SL. J Biomed Mater Res 1991;25:341–56.
[5] Lambda NMK, Woodhouse KA, Cooper SL. Polyurethanes in biomedical applications. Boca Raton: CRC Press; 1998.
[6] Martin DJ, Warren LAP, Gunatillake PA, McCarthy SJ, Meijs GF, Schindhelm K. Biomaterials 2000;21:1021–9.
[7] Huh DS, Cooper SL. Polym Eng Sci 1971;11:369–76.
[8] Christenson EM, Anderson JM, Hittner A. Corros Eng Sci Technol 2007;42:312–23.
[9] Briganti E, Losi P, Raffi A, Scoccianti M, Munao A, Soldani G. J Mater Sci Mater Med 2006;17:259–66.
[10] Gunatillake PA, Meijs GF, McCarthy SJ, Adhikari R. J Appl Polym Sci 2000;76:2026–40.
[11] Hernandez R, Weksler J, Padsalgikar A, Runt J. Macromolecules 2007;40:5441–9.
[12] Simmons A, Hyvarinen J, Odell RA, Martin DJ, Gunatillake PA, Noble KR, et al. Biomaterials 2004;25:4887–900.
[13] Simmons A, Hyvarinen J, Poole-Warren L. Biomaterials 2006;27:4484–97.
[14] Yu X-H, Nagarajan MR, Grasel TG, Gibson PE, Cooper SL. J Polym Sci Polym Phys Ed 1985;23:2319–38.
[15] Adhikari R, Gunatillake PA, McCarthy SJ, Meijs CF. J Appl Polym Sci 2000;78:1071–82.
[16] Adhikari R, Gunatillake PA, McCarthy SJ, Meijs GF. J Appl Polym Sci 2002;83:736–46.
[17] Lin YH, Chou NK, Chen KF, Ho GH, Chang CH, Wang SS, et al. Polym Int 2007;56:1415–22.
[18] Russell TP, Lin JS, Spooner S, Wignall GD. J Appl Crystallogr 1988;21:629–38.
[19] Sheth JP, Wilkes GL, Fornof AR, Long TE, Yilgor I. Macromolecules 2005;38:5681–5.
[20] Das S, Yilgor I, Yilgor E, Wilkes GL. Polymer 2008;49:174–9.
[21] Garrett JT, Siedlecki CA, Runt J. Macromolecules 2001;34:7066–70.
[22] Ponkitwitoon S, Hernandez R, Choi, T, Weksler J, Padsalgikar A, Runt J. Polymer, submitted for publication.
[23] Wang FC, Feve M, Lam TM, Pascault JP. J Polym Sci Part B Polym Phys 1994;32:1315–20.
[24] Sung CSP, Schneider NS. Macromolecules 1975;8:68–73.
[25] Coleman MM, Lee KH, Skrovanek DJ, Painter PC. Macromolecules 1986;19:2149–57.
[26] Bonart R, Muller EH. J Macromol Sci Phys 1974;B10:345–57.
[27] Bonart R, Muller EH. J Macromol Sci Phys 1974;B10:177–89.
[28] Leung LM, Koberstein JT. J Polym Sci Polym Phys Ed 1985;23:1883–913.
[29] Tyagi D, McGrath JE, Wilkes GL. Polym Eng Sci 1986;26:1371–98.
[30] Garrett JT, Runt J, Lin JS. Macromolecules 2000;33:6353–9.
[31] Wu W. Polym Bull 1982;23:1907–12.
[32] Koberstein JT, Stein RS. J Polym Sci Part B Polym Phys 1983;21:1439–72.
[33] Visser SA, Cooper SL. Macromolecules 1991;24:2584–93.
[34] Visser SA, Pruckmayr G, Cooper SL. Macromolecules 1991;24:6769–75.
[35] Yarusso DJ, Cooper SL. Macromolecules 1983;16:1871–80.